Bioorganic & Medicinal Chemistry 18 (2010) 5400–5412

Contents lists available at ScienceDirect

Bioorganic & Medicinal Chemistry

journal homepage: www.elsevier.com/locate/bmc

Development of a new radioligand for cholecystokinin receptor subtype 2 scintigraphy: From molecular modeling to in vivo evaluation

Séverine Brillouet [a,e,†], Sandra Dorbes [a,†], Frédéric Courbon [a,e,f], Claude Picard [c,d], Jean Pierre Delord [g], Eric Benoist [c,d], Marc Poirot [a,b], Béatrice Mestre-Voegtlé [c,d,*], Sandrine Silvente-Poirot [a,b,*]

[a] *INSERM 563, Equipe Marc Poirot «Métabolisme, Oncogenèse et Différenciation cellulaire», CPTP, Toulouse, France*
[b] *Université Paul Sabatier Toulouse III, Toulouse, France*
[c] *CNRS;Laboratoire de Synthèse et Physico-Chimie de Molécules d'Intérêt Biologique, SPCMIB, UMR-5068, Toulouse, France*
[d] *Université Paul Sabatier Toulouse III, Laboratoire de Synthèse et Physico-Chimie de Molécules d'Intérêt Biologique, SPCMIB, Toulouse, France*
[e] *Département d'Imagerie Médicale, Institut Claudius Regaud, Toulouse, France*
[f] *CHU Rangueil, Toulouse, France*
[g] *Institut Claudius Regaud et EA3035 Laboratoire de Pharmacologie Clinique et Expérimentale des Médicaments Anticancéreux, Toulouse, France*

ARTICLE INFO

Article history:
Received 9 March 2010
Revised 11 May 2010
Accepted 12 May 2010
Available online 19 May 2010

Keywords:
Metal chelate
Gastrin receptor
^{111}Indium
Metal conjugate
SPECT
Cancer

ABSTRACT

To improve the targeting to tumors expressing the cholecystokinin receptor subtype 2 (CCK2R) with limited kidney uptake, we synthesized a novel cholecystokinin C-terminal tetrapeptide (CCK4)-based derivative conjugated to an original bipyridine-chelator (BPCA), ^{111}In-BPCA-(Ahx)$_2$-CCK4. To our knowledge this is the first CCK4-based radioligand that presents a high affinity for the CCK2R, a high and specific tumor uptake, a low renal accumulation and a very good visualization of tumors in vivo compared with an internal control, ^{111}Indium-*trans*-cyclohexyldiethylenetriaminepenta-acetic acid-cholecystokinin octapeptide (^{111}In-CHX-A″-DTPA-CCK8). These properties make ^{111}In-BPCA-(Ahx)$_2$-CCK4, a promising candidate for imaging and peptide receptor radionuclide therapy of CCK2R positive tumors.

1. Introduction

Peptides as tools to diagnose and treat human cancers have been the focus of interest over recent years in nuclear medicine.[1,2] The successful development of radiolabeled somatostatin analogs as radiopharmaceuticals has opened up new horizons in nuclear oncology and patient management. ^{111}In-DTPA-[D-Phe]-octreotide (octreoscan) is the first radiopeptide to obtain regulatory approval in Europe and the United States for imaging somatostatin receptors.[3,4] Whereas somatostatin receptor scintigraphy has proved to be a valuable tool for evaluating the staging of gastroenteropancreatic tumors, its sensitivity for some neuroendocrine tumors is limited. Indeed, either the somatostatin receptor subtype 2 (sst2) are not expressed in all tumors and metastases, or the expression of these receptors can change during the evolution of the pathology.[5–7] The relatively recent discovery that many tumors overexpress other peptide receptors, such as the cholecystokinin receptor subtype 2 (CCK2R), has opened up a new area of research for the diagnostic and radiotherapy of cancers.[8]

The CCK2R is a G protein-coupled receptor that mediates important physiological functions by binding cholecystokinin (CCK) and gastrin peptides with high affinity. CCK and gastrin are two evolutionarily related families of regulatory peptides that exist in multiple forms. Both peptides have an identical carboxyl-terminal amidated pentapeptide sequence but differ in the N-terminal part of the peptide sequence and in the position of a tyrosine sulfate at the seventh position (CCK) versus a variably sulfated tyrosine in the sixth position (gastrin) from the carboxyl. The CCK2R and the CCK1R, the other receptor subtype, have an equally high affinity for sulfated CCK peptides, while only the CCK2R has a high affinity for gastrin, non-sulfated CCK and CCK4, the C-terminal

Abbreviations: CCK, cholecystokinin; CCK2R, cholecystokinin 2 receptor; CHX-A″-DTPA, *trans*-cyclohexyldiethylenetriaminepenta-acetic acid; BPCA, bipyridine chelating agent; Ahx, 6-aminohexanoic acid.

* Corresponding authors. Address: INSERM U563, 20-24 rue du Pont-St-Pierre, 31052 Toulouse, Cedex, France. Tel.: +33 561424648; fax: +33 561424631 (S.S.-P.). UMR-CNRS 5068, Université Paul Sabatier, 118 route de Narbonne, 31062 Toulouse, Cedex, France. Tel.: +33 561556288; fax: +33 561556011 (B.M.-V.).
E-mail addresses: mestre@chimie.ups-tlse.fr (B. Mestre-Voegtlé), poirot.sandrine@hotmail.fr (S. Silvente-Poirot).
† Both authors equally contributed to the work and should be considered as first authors.

0968-0896/$ - see front matter © 2010 Elsevier Ltd. All rights reserved.
doi:10.1016/j.bmc.2010.05.031

amidated tetrapeptide of CCK, Trp-Met-Asp-Phe-NH_2. CCK4 represents the minimal active agonist that has nanomolar affinity for the CCK2R.[9]

CCK2R expression has been reported on malignant adenocarcinomas arising within all areas of the gastrointestinal tract mucosa, hepatomas and colorectal liver metastases.[10–13] The CCK2R is also highly expressed in several neuroendocrine tumors whereas it is not present in the corresponding normal tissues.[14] A permanent activation of the CCK2R by an autocrine loop has been shown to promote cell growth.[11,15–18] We have developed a model of permanent activation of the CCK2R by stably expressing a constitutively active mutant of the CCK2R in NIH-3T3 cells resulting from the mutation of the residue Glu 151 to an Ala (CCK2R-E151A cells).[19] The expression of the CCK2R-E151A mutant in NIH-3T3 cells induced the formation of tumors in nude mice.[19] This tumor model was used to characterize the signaling pathways involved in cell proliferation and invasion.[20]

Comparison of gastrin and somatostatin receptor scintigraphies in patients with neuroendocrine tumors indicated that the CCK2R receptor scintigraphy could be an additional imaging modality.[6,21] Gotthardt et al. showed that gastrin receptor scintigraphy in metastasised/recurrent medullary thyroid carcinoma (MTC) patients had a higher tumor detection rate (94%) than somatostatin receptor scintigraphy (40%) and ^{18}F-FDG positron emission tomography (67%).[21] Minigastrin, a truncated form of gastrin with 13 amino acids from the C-terminus, radiolabeled with ^{111}In (^{111}In-DTPA-minigastrin) was used in a clinical study including 75 metastatic MTC patients: 43 suffered of known and 32 of occult disease. All known tumor lesions were visualized and at least one lesion was detected in 29 patients with occult disease (patient-based sensitivity 91%).[5] To test the efficacy of minigastrin in peptide receptor radionuclide therapy (PRRT), eight patients with metastatic disease were injected with ^{90}Y radiolabeled minigastrin. The results were promising: two partial remissions and four stabilizations of previously rapidly progressing disease were observed. However, the high tumor accumulation of minigastrin radioligand was associated with a high kidney uptake which was at the origin of the nephrotoxicity observed in 2 patients.[5,22] High kidney uptake (concentrations of radioactivity accumulated in the kidneys) and high kidney retention (fraction of the radioactivity that is trapped in the cortical proximal tubules) are undesirable as the kidney is a dose limiting organ in PRRT. In contrast, cholecystokinin analogs, such as CCK8, showed moderate to low tumor accumulation in vivo but with a lower kidney uptake compared with gastrin compounds.[23] Different chelators have been tested for these purposes. The acyclic chelator diethylenetriamine-pentaacetic acid (DTPA) has been used, but the [^{90}Y-DTPA] corresponding complexes were not stable enough for targeted radionuclide therapy.[24] A DTPA derivative of D-Glu-minigastrin has also been synthesized to increase the efficiency of indium and yttrium chelation[25] but the low tumor-to-kidney ratio restricted its therapeutic use.[5,22,26] DOTA (tetra-azacyclododecane-*N*,*N*′,*N*″,*N*‴-tetra-acetate) is the most frequently used chelator for radiopeptide therapy because it forms stable complexes with a broad range of metallic ions such as ^{111}In, $^{86/90}$Y. However, it is sensitive to metal impurities and requires heating steps that can affect the molecular integrity of the ligand. Minigastrins were coupled with macrocyclic chelators like DOTA to increase the corresponding stability of the complexes and the poly-Glu sequence in the N-terminal part of the peptide removed to increase the tumor-to-kidney ratio that was low. Reducing the number of glutamates increased the tumor-to-kidney ratio but resulted in lower metabolic stability.[27] These different studies show that the nature of the peptidic part of the ligand may influence the renal retention. They also demonstrate that the choice of the chelator is crucial to preserve the integrity of the peptide during the radiolabeling step as well as to give a stable radiolabeled peptide to ensure efficient transport of the radionuclide to the targeted tumor.

In this context, with the perspective of improving the targeting of the CCK2R for the diagnosis and PRRT of tumors with limited kidney retention, we synthesized a new radiochemical. This was achieved by using an original pre-organized acyclic chelator (BPCA, Fig. 1) and by modifying the peptidic part of the ligand.

The BPCA chelator was constructed on the basis of amino-carboxylate units combined with a modified 2,2′-bipyridine chromophore.[28] This bifunctional chelating agent is composed of (i) a chelating site adequate for efficient complexation of lanthanide and related ions such as In(III) and (ii) a reactive group, in position 4 of its bis-heterocycle, available for its bioconjugation.[29] Moreover, the chelation of gadolinium by BPCA produces a magnetic probe for magnetic resonance imaging (MRI) applications. Actually, the $1/T_1$ proton relaxivity at 20 MHz and 37 °C (r_1 = 4.4 s^{-1} mM^{-1}) of the Gd(III) chelate was found to be comparable to those of the clinically used MRI agents Gd-DTPA and Gd-DOTA.[‡] Additionally, with some lanthanides, such as luminescent europium and terbium, this bifunctional chelating agent gives complexes that show special luminescent properties. In particular, these complexes with long-lived luminescences are of major interest for doing experiments based on time-resolved fluorescence spectroscopy.[28,30] Thus this chelator potentially offers a wide range of imaging modalities. In the present study, in order to evaluate BPCA, it was compared with a preorganized cyclohexyl derivative of DTPA (CHX-A″-DTPA, *trans*-cyclohexyldiethylenetriaminepenta-acetic acid)[31] that can form at room temperature stable metal complexes with γ (^{111}In), Auger (^{111}In), β$^-$ (^{177}Lu, ^{90}Y), and β$^+$ (^{86}Y) emitters.

Since low renal uptake was observed with CCK peptides, BPCA and CHX-A″-DTPA chelators were coupled to a CCK4-based peptide. The molecular model of the CCK2R occupied by CCK that we built and validated experimentally[32–35] was used to evaluate in silico the steric hindrance that may be generated by the chelator in the receptor binding site and the modifications needed in the peptide sequence to maintain an intact binding site in the CCK2R.

The evaluation of these radioligands (Fig. 1) was carried out in nude mice bearing E151A-CCK2R tumors[19] and compared with the reference ^{111}In-CHX-A″-DTPA-CCK8. We present here the ability of BPCA to vectorize ^{111}In for CCK2R scintigraphy through its conjugation to a CCK4-based ligand.

2. Results

2.1. Molecular modeling of the CCK2R occupied by In-BPCA-(Ahx)$_n$-CCK4 (*n* = 0, 1, 2)

Since low renal uptake was observed with CCK peptide family compared with gastrin peptides, the C-terminal tetrapeptide of CCK (CCK4) that represents the minimal sequence with nanomolar affinity for the CCK2R was chosen as the starting motif.[9] Since metal complexes are voluminous and thus may affect the high affinity binding of the CCK peptide by introducing steric hindrance in the binding site of the CCK2R, we used the cholecystokinin C-terminal nanopeptide (CCK9)-occupied CCK2R molecular model (CCK9-CCK2R) that we have built and validated experimentally[32,33] to evaluate such effects and the modifications needed in the peptide sequence to maintain an intact binding site. Indeed, Behr et al. reported that CCK4 coupled to radioiodinated Bolton Hunter reagent had 100-fold less affinity for the receptor, while the affinities of radioiodinated CCK8 (the C-terminal octapeptide of CCK) or minig-

[‡] Leygue, N.; Laurent, S.; Vander Elst, L.; Muller, R.N.; Picard, C., personal communication.

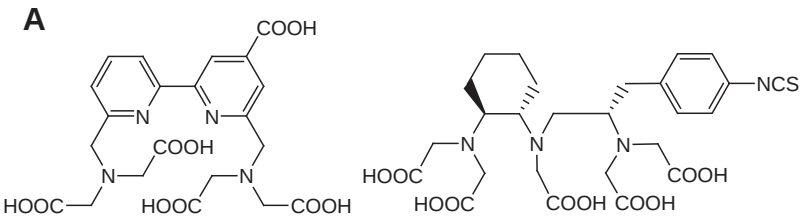

B

CCK8	Asp-Tyr-Met-Gly-Trp-Nle[b]-Asp-Phe-NH_2
(Ahx[a])$_2$-CCK4	Ahx-Ahx-Trp-Nle[b]-Asp-Phe-NH_2

[a]Ahx means 6-aminohexanoic acid, [b]Nle means Norleucine

Figure 1. Chemical structures. (A) Structures of the bifunctional chelating agents: bipyridine chelating agent (BPCA) and isothiocyanate derivative of CHX-A″-DTPA; (B) sequences of $(Ahx)_2$-CCK4 and CCK8 peptides.

astrin derivatives were not affected.[22,36] In-BPCA can be compared to a sphere of 12 Å diameter. This is higher than that of the binding site pocket of the CCK2R whose highest diameter is approximately 10 Å (Fig. 2, indicated by dotted line), indicating that In-BPCA would generate steric hindrance in the binding site if it was directly coupled at the N-terminus of the CCK peptide. In our molecular model, the binding site of CCK is located at the bottom of a cone of 14 Å long and involves residues in the transmembrane domains (Y189 (TM4), N358 (TM6), W351 (TM6), H381 (TM7), Y385 (TM7)), as well as in the first and second extracellular loops (F120 (ECL1), H207 (ECL2)) of the CCK2R.[32–35] A possibility to avoid a deformation in the binding site was to introduce a spacer with a length higher or equal to 14 Å between CCK4 and BPCA to maintain it outside the binding pocket. We chose as spacer 6-aminohexanoic acid that has the advantage of adopting an extended conformation. We determined that two linked 6-aminohexanoic acids (Ahx) coupled at the N-terminus of CCK4 should be necessary to reach this distance. As controls, we tested the same peptide with 0 or 1 Ahx spacer (In-BPCA-$(Ahx)_0$-CCK4 and In-BPCA-$(Ahx)_1$-CCK4). A dynamic simulation of the CCK2R occupied by In-BPCA-$(Ahx)_2$-CCK4 resulted in a thermodynamically stable complex that maintained In-BPCA outside the receptor with no gross deformation in the binding site (Fig. 2 and Table 1). Similar experiments performed with In-BPCA-$(Ahx)_1$-CCK4 showed an electrostatic interaction between one of the carboxylates of BPCA and R57 (TM1) (Table 1). In addition, we measured that the distance between the imidazole of H207 (ECL2) and the carboxylate side chain of Asp[8] of CCK was increased by 2.8 Å in the In-BPCA-$(Ahx)_1$-CCK4-CCK2R model compared with that measured in the CCK9-CCK2R model (4.7 vs 1.9 Å), indicating that the electrostatic interaction was weaker than in the CCK9-CCK2R model (Table 1). Moreover, the hydrogen bond (distance 2 Å) linking the oxygen atom of the carboxamide functional group of N358 with a proton of the NH_2 group of the C-terminal amide of CCK9 was found disrupted (3.8 vs 1.9 Å) (Table 1). Similar experiments performed with In-BPCA-$(Ahx)_0$-CCK4 resulted in a gross deformation of the binding pocket of the ligand (not shown). Together, these data indicated that only In-BPCA-$(Ahx)_2$-CCK4 should maintain an intact binding site. Based on these results, ^{111}In-BPCA-$(Ahx)_2$-CCK4 was synthesized and evaluated in vitro and in vivo in comparison with ^{111}In-CHX-A″-DTPA-$(Ahx)_2$-CCK4 and ^{111}In-CHX-A″-DTPA-$(Ahx)_2$-CCK8 radioligands.

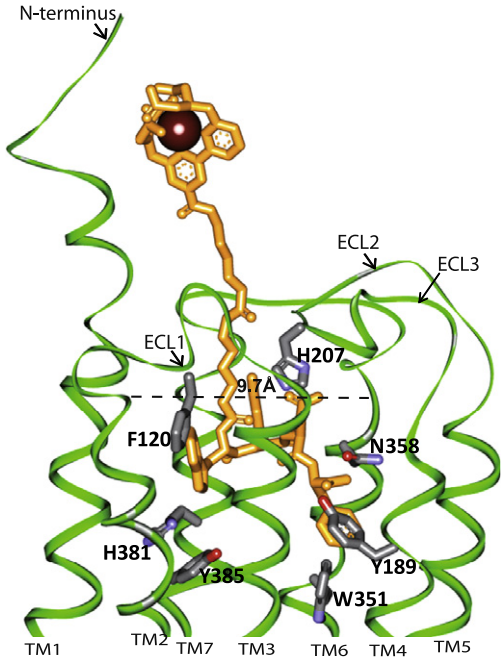

Figure 2. Molecular modeling. Side view of the three-dimensional model of the In-BPCA-$(Ahx)_2$-CCK4-CCK2R complex. The model was built as described in Section 4. The side chains of amino acids of the CCK2R in interaction with the C-terminal amino acids of CCK4 are in gray and their location in the CCK2R are indicated by a number. The seven transmembrane (TM) alpha helices and the extracellular loops (ECL) of the CCK2R are in green and are numbered (1, 2…) from the N-terminus to the C-terminus of the receptor as indicated in the figure. Oxygen atoms are in red and nitrogen atoms are in blue. The ligand is in yellow and indium in brown. The binding site of CCK involves amino acids of the CCK2R located in the seven transmembrane (TM) helices: Y189 (TM4), N358 (TM6), W351 (TM6), H381 (TM7), Y385 (TM7), as well as amino acids located in the first and second extracellular loops: F120 (ECL1), H207 (ECL2).[32–35] The dotted line in the molecular model indicated the highest diameter of the ligand binding pocket (9.7 Å). No gross deformation of the CCK binding site was observed in this model compared with the CCK9-CCK2R model published previously[32–35] and Table 1.

2.2. Synthesis

The BPCA bifunctional chelating agent (Fig. 1) was synthesized in its protected form as described previously.[28] In order to proceed to a specific coupling reaction of this chelating agent at the N-terminus of the $(Ahx)_2$-CCK4 peptide, it was partially unprotected through a selective hydrolysis of its methyl ester group (Fig. 3). *tert*-Butyl protection of the carboxylate chelating functions ensures that no unwanted coupling reactions occur on these chelating positions. Characterization and confirmation of the structure of the semi-protected BPCA were obtained by ^{1}H NMR, ^{13}C NMR and electrospray mass spectrometry.

Table 1
Molecular modeling

CCK2R/ligand[a]	Interaction[b]	CCK9-CCK2R[c] (Å)	In-BPCA-$(Ahx)_1$-CCK4-CCK2R[d] (Å)	In-BPCA-$(Ahx)_2$-CCK4-CCK2R[e] (Å)
H207/Asp^8	Electrostatic	1.9	4.7	3.2
F120/Trp^6	Aromatic	7.6	6.8	7.0
Y189/Phe^9NH_2	Aromatic	3.4	2.6	3.6
Y189/Phe^9NH_2	Hydrogen	3.3	2.1	1.7
N358/Phe^9NH_2	Hydrogen	1.9	3.8	1.9
Y385/Trp^6	Aromatic	4.4	5.5	5.7
H381/Trp^6	Aromatic	3.7	5.5	5.2
W351/Trp^6	Aromatic	3.3	5.2	3.2
R57/BPCA	Electrostatic	—	2.2 (BPCA)	—

In ([a]) are indicated the amino acids of the receptor (CCK2R) in interaction with essential amino acids of the ligand or with BPCA (ligand). In ([b]) are indicated the type of interaction involved between the amino acids of the receptor and the ligand (amino acids or BPCA). In ([c,d,e]) are indicated the distance (in Å) between these pair of residues in the three molecular models: [c]CCK9-CCK2R, [d]In-BPCA-$(Ahx)_1$-CCK4-CCK2R and [e]In-BPCA-$(Ahx)_2$-CCK4-CCK2R. The data indicate that different modifications in the binding site occurred in the In-BPCA-$(Ahx)_1$-CCK4-CCK2R model compared with the CCK9-CCK2R model: the electrostatic interaction between the imidazole of H207 and the carboxylate side chain of Asp^8 of CCK was weaker in this model (4.7 vs 1.9 Å), the hydrogen bond linking N358 with the C-terminal amide of CCK9 was disrupted (3.8 vs 1.9 Å) and one of the carboxylates of BPCA interacted through an electrostatic interaction with R57. In contrast, in the In-BPCA-$(Ahx)_2$-CCK4-CCK2R model, no gross deformation in the binding site was observed compared with the CCK9-CCK2R model and In-BPCA was not in interaction with residues of the CCK2R indicating that In-BPCA-$(Ahx)_2$-CCK4 maintains an intact binding site.

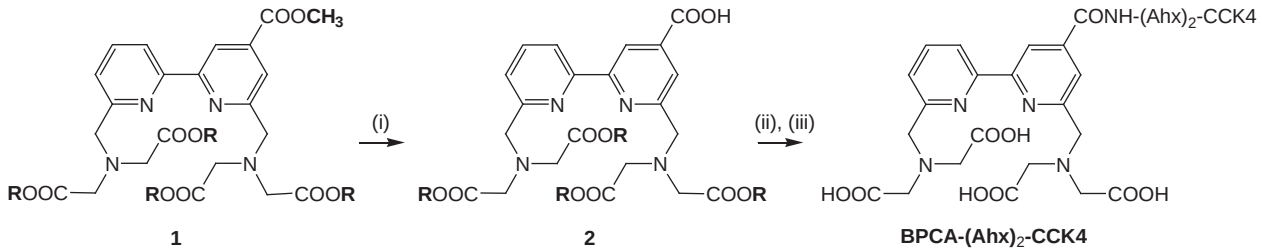

Figure 3. Schematic representation of the synthesis of the BPCA-$(Ahx)_2$-CCK4 conjugate. R = *t*Bu; (i) K_2CO_3, H_2O/CH_3OH 1:2; (ii) $(Ahx)_2$-CCK4, CDI, DMF; (iii) TFA/CH_2Cl_2 1:1, EDT, TIS.

Conjugation reactions involving CHX-A″-DTPA were carried out by reaction of its isothiocyanate reactive group with the N-terminus positions of both $(Ahx)_2$-CCK4 and CCK8 peptides. These reactions were performed in anhydrous dimethylformamide (DMF), with 2 equiv of SCN-CHX-A″-DTPA and 10 equiv of triethylamine compared with the peptide. With such coupling conditions, the reactions were quantitative as shown by the disappearance of the starting peptidic material, observed by chromatographic monitoring of the reactions.

The synthesis of BPCA-$(Ahx)_2$-CCK4 conjugate (Fig. 3) comprised two steps: (i) the formation of a peptide bond between the activated carboxylic acid group of protected BPCA and the terminal amino function of the peptide, using 1,1′-carbonyldiimidazole (CDI) in anhydrous DMF at 40 °C. (ii) The resulting coupling product was then treated with trifluoroacetic acid (TFA) containing scavengers such as tris-isopropylsilane (TIS) and ethanedithiol (EDT) to avoid alkylation of the tryptophan unit which occurs when releasing carboxylate functions from *tert*-butyl protective groups. Every conjugation reaction was performed on a small-scale format: typically, 1–10 micromoles of peptide were used in the coupling reactions. All samples of conjugates were purified by High-Performance Liquid Chromatography (HPLC). The yields of synthesis for individual products, along with analytical data from HPLC and electron spray ionization (ESI) results are compiled in Table 2.

Following the HPLC purification, we obtained levels of purity for each conjugate higher than 95%. The chemical purities of conjugates were measured on the basis of their UV monitored chromatographic profiles: a major peak relative to the compound of interest was usually accompanied by minor peaks which, accordingly to their UV spectra and ESI mass spectra, were traces of adducts and/or chelates with ions such as Na^+, K^+, Fe^{3+} as it was seen with the conjugate BCPA-$(Ahx)_2$-CCK4. For this reason, treatment with a chelating resin (Chelex 100® resin) was systematically carried out prior to the radiolabeling of the peptidic conjugates. These treatments were efficient at further purifying the conjugates as demonstrated by HPLC elution of treated samples (results not shown).

Table 2
Analytical data of the conjugates

Conjugates	% Purity[a]	% Yield	ESI, *m*/*z*, $[M+H^+]$ calculated	ESI, *m*/*z*, $[M+H^+]$	HPLC[b], T_r (min)
CHX-A″-DTPA-CCK8	96	33	1657.6	1658.4	30.4
CHX-A″-DTPA-$(Ahx)_2$-CCK4	95	67	1399.7	1400.1	32.5
BPCA-$(Ahx)_2$-CCK4	96[c]	20[d]	1277.6	1277.8	23.9

Ahx means 6-aminohexanoic acid.
[a] Purity was determined by HPLC.
[b] RP-HPLC with UV detection (280 nm). Column: Phenomenex Luna C18(2), 5 μ, 250 × 4.6 mm; solvent H_2O containing 0.1% TFA (solvent A) and acetonitrile (solvent B); linear gradient, 15–40% B in 30 min and 40–60% B in 5 min; flow rate: 1 ml/min.
[c] The purity was determined after the Chelex treatment.
[d] Overall yield for two steps.

2.3. $^{113/115}$In-labeling of peptide conjugates

The assays were performed at analytical scales to demonstrate the ability of the peptide conjugates to rapidly form stable complexes with indium (In). These assays were performed with naturally occurring $^{113/115}$In, they were followed by UV monitored HPLC. The complexation reactions took place in a 0.1 M sodium acetate buffer pH 5 at room temperature with small amounts of

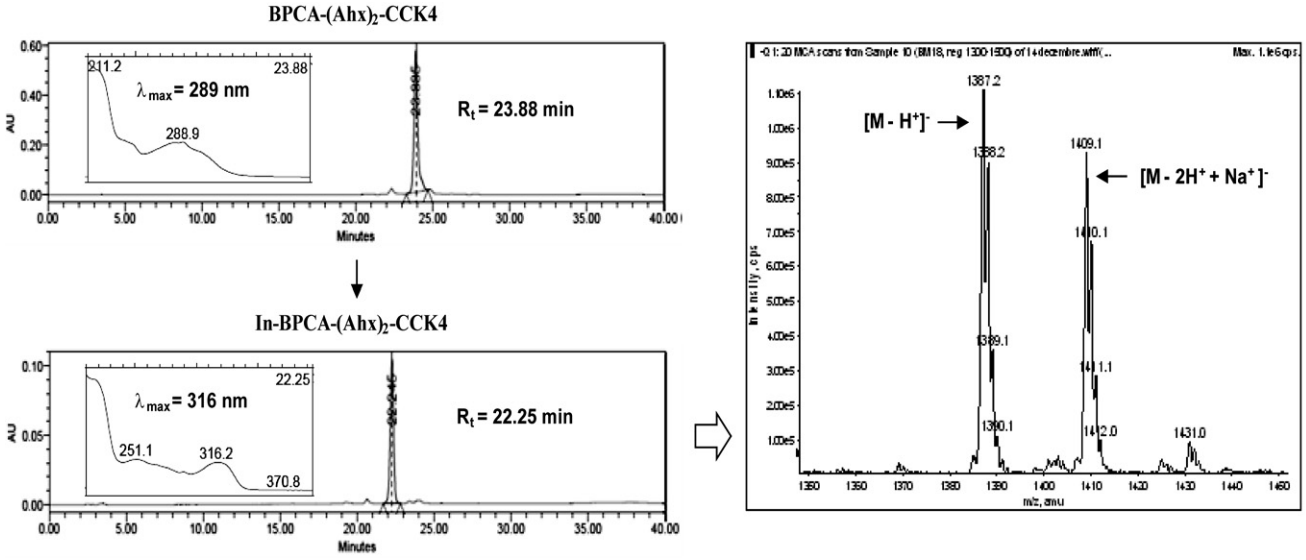

Figure 4. Reversed-phase HPLC traces and UV spectra of the BPCA-$(Ahx)_2$-CCK4 conjugate (R_t = 23.88 min) and the corresponding In-BPCA-$(Ahx)_2$-CCK4 complex (R_t = 22.25 min) for which the ESI mass spectrum is shown in the right part of the figure. For chromatographic conditions, see Section 4.

peptide conjugates (0.04 μmol) and by the addition of 1 equiv of $^{113/115}In^{3+}$ ($InCl_3.4H_2O$, 0.04 μmol) compared with the conjugate. As shown in Figure 4, the BPCA-$(Ahx)_2$-CCK4 conjugate characterized by a retention time of 23.88 min, has disappeared totally from the middle reaction after 1 h. Indeed, at this time of reaction, the chromatogram shows the corresponding $^{113/115}$In-BPCA-$(Ahx)_2$-CCK4 metal chelate: the indium labeled conjugate has a retention time of 22.25 min and in addition it has a characteristic UV absorption (λ_{max} = 316 nm instead of 289 nm before complexation). Actually, upon complexation, the band at 316 nm attributed to π–π^* transitions centered on the 2,2′-bipyridine group is shifted by 27 nm toward longer wavelength by comparison to the band of the chelator at 289 nm. This shift of the absorption to lower energy from the chelator to its In^{3+} complex is indicative of a perturbation produced by the coordinated metallic ion. This bathochromic shift was previously reported for similar complexes of lanthanide ions.[37]

The indium labeled conjugate was then examined by ESI mass analysis which confirmed its formation and its stability under analytical conditions (Fig. 4). Similar results were obtained for CHX-A″-DTPA-$(Ahx)_2$-CCK4: the conjugate (R_t = 30.00 min) has disappeared 1 h after addition of $^{113/115}$In-chloride leading to a single peak of the corresponding indium labeled conjugate which has a retention time R_t = 27.50 min. Then following the procedure described above, the In-labeled conjugates: $^{113/115}$In-CHX-A″-DTPA-CCK8, $^{113/115}$In-CHX-A″-DTPA-$(Ahx)_2$-CCK4, and $^{113/115}$In-BCPA-$(Ahx)_2$-CCK4, were prepared for the in vitro evaluation of their affinity to the CCK2 receptor.

2.4. Stability of the $^{113/115}$In-complexes to transchelation

$^{113/115}$In-BPCA and $^{113/115}$In-CHX-A″-DTPA were incubated in a solution of human transferrin (0.25 g/100 ml) in a 50 mM HEPES buffer pH 7.3 to determine the relative stability of both complexes to transchelation.[38] The assessment of the stability of the complexes was performed by following their disappearance as a function of the time of incubation. The results showed that $^{113/115}$In-BPCA appeared more resistant to transchelation by the plasma protein than $^{113/115}$In-CHX-A″-DTPA. Indeed, after 2.5 h of incubation at 37 °C in the medium containing transferrin, 89% of $^{113/115}$In-BPCA remained whereas only 45% of $^{113/115}$In-CHX-A″-DTPA was still intact. After 5.5 h under the same conditions, 71% of $^{113/115}$In-BPCA was present while only 23% of the indium complex of CHX-A″-DTPA resisted to the probable transchelation of the transferrin.

2.5. Radiolabeling and quality control of the radiometal conjugates

Rapid and efficient labeling was obtained as early as 15 min after the addition of ^{111}In to the CCK4–peptide conjugates. For each of them, a single peak corresponding to the ^{111}In-peptide conjugate was determined by Instant Thin-Layer Chromatography (ITLC) indicating a radiochemical purity (RCP) >95% that did not require additional post-labeling purification (Fig. 5). The percentage of ^{111}In free was always found to be <5% during ITLC analysis. The radiochemical purity tested at 15 min, 30 min, 1 h, 2 h, 4 h, 7 h, and 24 h was always >95% showing a high stability of the radiocomplexes. The specific activities of the radiochemicals ranged from 6.5 to 10 GBq/μmol.

2.6. Pharmacological properties of the $^{113/115}$In-labeled conjugates

To determine whether the peptide conjugates and the corresponding $^{113/115}$In-labeled conjugates had conserved an agonist activity, we measured their potencies (EC_{50}) and efficacies (E_{max}) in inducing the production of inositol phosphates after stimulation of cells expressing the CCK2R. Their activities were compared with CCK8, the endogenous agonist of the CCK2R. As shown in Table 3, all the peptide conjugates and $^{113/115}$In-labeled conjugates displayed a potency (EC_{50}) in the nanomolar range and an efficacy to stimulate maximal IP production (E_{max}) similar to the endogenous agonist indicating that the CHX-A″-DTPA and BPCA chelators did not modify the affinity and activity of the compounds. The data also indicated that these compounds are full agonists since they induced a similar maximal IP production (E_{max}) than the endogenous ligand. To determine the affinity and selectivity of ^{111}In-BPCA-$(Ahx)_2$-CCK4 for the CCK2R, saturation binding experiments were performed on cells expressing either the CCK2R or the CCK1R. ^{111}In-BPCA-$(Ahx)_2$-CCK4 showed high affinity for the CCK2R expressed transiently in COS cells (K_d = 3.40 ± 0.46 nM, n = 3) as well as for the constitutively active mutant of the CCK2R stably expressed in NIH-3T3 cells (K_d = 1.21 ± 0.02 nM, n = 3). In contrast,

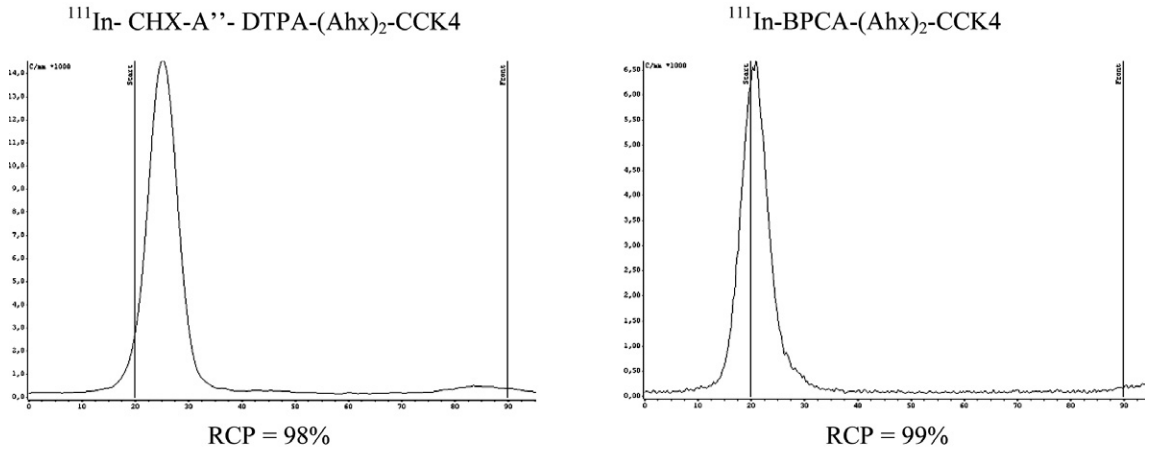

Figure 5. Determination of the radiochemical purity of radiolabeled ligands. A single peak corresponding to ^{111}In-CHX-A″-DTPA-(Ahx)$_2$-CCK4 or ^{111}In-BPCA-(Ahx)$_2$-CCK4 was visualized by the ITLC method using 0.1 M pH 5 sodium citrate buffer as eluent. The radiochemical purity (RCP) was determined using the radiochromatograph Mini-Gita. Free ^{111}In was found at the solvent front and was always <5%.

Table 3
Potencies of the conjugates for the WT-CCK2R transiently expressed in COS cells

	Conjugates						
	CCK8	CHX-A″-DTPA-CCK8	CHX-A″-DTPA-(Ahx)$_2$-CCK4	BPCA-(Ahx)$_2$-CCK4	In-CHX-A″-DTPA-CCK8	In-CHX-A″-DTPA-(Ahx)$_2$-CCK4	In-BPCA-(Ahx)$_2$-CCK4
EC_{50} (nM)	0.40 ± 0.09	0.43 ± 0.37	0.45 ± 0.20	0.81 ± 0.04	1.13 ± 0.67	1.01 ± 0.18	1.33 ± 0.65
E_{max} (%)	100	100	100	100	100	100	100

Ahx means 6-aminohexanoic acid.
The potencies (EC_{50}) were calculated from the total IP production concentration–response curves stimulated by the indicated ligands and the efficacies (E_{max}) to stimulate IP production were expressed as the percentages of the maximal increase obtained with 1 μM CCK-8 ns. EC_{50} values (mean ± SD) and E_{max} were determined from three experiments performed in duplicate.

no binding was measured in COS cells expressing the CCK1R, indicating that ^{111}In-BPCA-(Ahx)$_2$-CCK4 was highly selective for the CCK2R. Radioligand stripping experiments were then performed to investigate the internalization of ^{111}In-BPCA-(Ahx)$_2$-CCK4. As shown in Figure 6, cells expressing the CCK2R internalized ^{111}In-BPCA-(Ahx)$_2$-CCK4 rapidly and to a high degree. Indeed, the internalization process reached a plateau after 15 min, with a maximal internalization of 94% of the total specific binding of ^{111}In-BPCA-(Ahx)$_2$-CCK4.

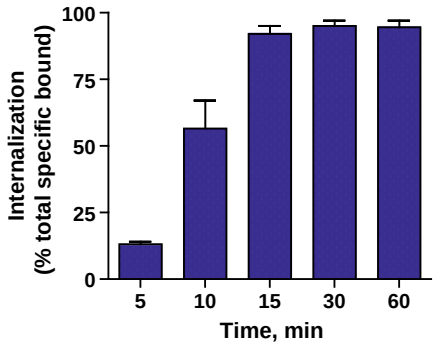

Figure 6. Internalization of ^{111}In-BPCA-(Ahx)$_2$-CCK4 in cells expressing the CCK2R. COS cells expressing the CCK2R were incubated with ^{111}In-BPCA-(Ahx)$_2$-CCK4 (100 kBq). At the indicated time points, cells were exposed to a 0.5 M KSCN solution. Internalized radioligand is defined as ^{111}In-BPCA-(Ahx)$_2$-CCK4 that could not be stripped by KSCN and is expressed as percentage of the total specific bound ^{111}In-BPCA-(Ahx)$_2$-CCK4 in control cells processed in parallel without the KSCN exposure. Each value represents the mean ± S.E. of three experiments performed in duplicate.

2.7. Biodistribution studies and tumor uptake of the radiometal conjugates in mice bearing E151A-CCK2R tumors

The results of the tissue biodistribution at different times (1 h, 4 h, and 24 h) after iv injection of the radioligands into nude mice with CCK2R-E151A tumor xenografts are shown in Figure 7, expressed as percentages of the injected dose per gram of tissue (% ID/g). For all radioligands and conditions, a fixed amount of radioligand (1 nmol, around 8 MBq) was injected in animals. As shown in Figure 7A, for all the radioligands, the biodistribution studies performed at 24 h after injection indicated that the major route of excretion was renal and biliary (transient gallbladder uptake with the transfer of radioactivity into the bowel). The results showed that the modification of the peptidic part of the ligand increased the tumor uptake since ^{111}In-CHX-A″-DTPA-(Ahx)$_2$-CCK4 had a threefold higher tumor uptake than the reference ^{111}In-CHX-A″-DTPA-CCK8 (Fig. 7A) and a tumor-to-muscle ratio of 2 (Table 4). The coupling of BPCA to the (Ahx)$_2$-CCK4 accentuated this effect. Indeed, a fourfold higher tumor accumulation was measured with ^{111}In-BPCA-(Ahx)$_2$-CCK4 compared with ^{111}In-CHX-A″-DTPA-CCK8 (Fig. 7A) and a tumor-to-muscle ratio of 4 was determined (Table 4). Interestingly, this enhanced tumor uptake was also associated with a low kidney uptake (less than 0.5% ID/g) and an increased tumor-to-kidney ratio (Fig. 7A and Table 4). For ^{111}In-CHX-A″-DTPA-(Ahx)$_2$-CCK4, there was a fourfold increase in the tumor-to-kidney ratio compared with the reference radioligand (0.12 vs 0.03, Table 4). For ^{111}In-BPCA-(Ahx)$_2$-CCK4, a tumor-to-kidney ratio of 0.2 was obtained that was sevenfold higher than that of ^{111}In-CHX-A″-DTPA-CCK8 and 1.8-fold better than ^{111}In- CHX-A″-DTPA-(Ahx)$_2$-CCK4 (Table 4). Importantly, the tumor-to-stomach ratio of ^{111}In-BPCA-(Ahx)$_2$-CCK4 was also in-

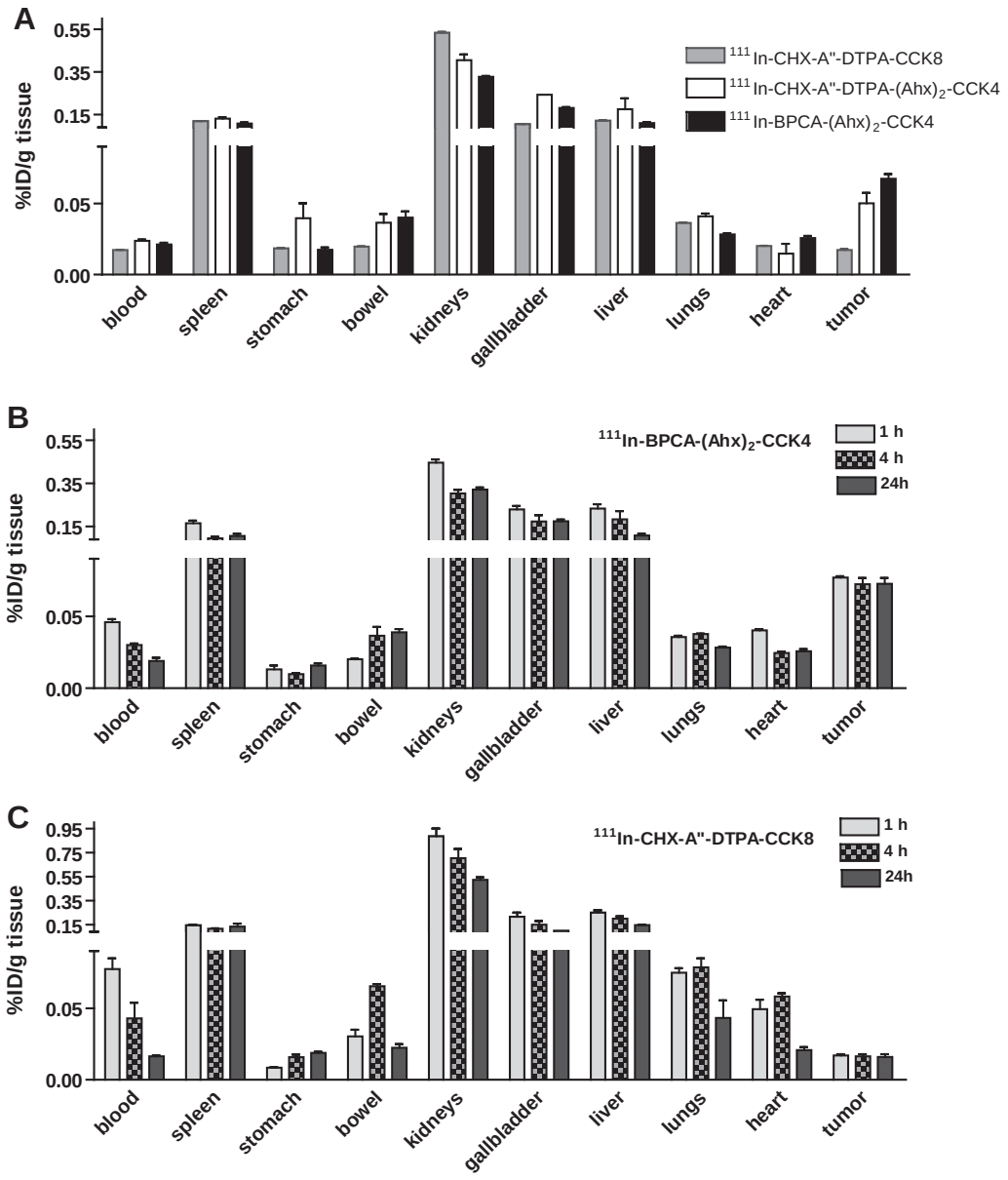

Figure 7. Biodistribution studies of the indicated ^{111}In-radioconjugates at different times post-injection into E151A-CCK2R tumor-bearing mice. The percentages of the injected dose per g of tissue (% ID/g) are expressed as mean ± SD of three to six experiments.

creased fourfold compared with that of ^{111}In- CHX-A″-DTPA-CCK8 while that of ^{111}In-CHX-A″-DTPA-$(Ahx)_2$-CCK4 was close to the reference (Table 4). Together these data show that the modification introduced into the peptidic part of the ligand as well as the coupling to BPCA improved the targeting to tumors and lowered it to the stomach, a CCK2R-expressing organ, while maintaining low kidney uptake. The biodistribution studies carried out at different times after injection of ^{111}In-BPCA-$(Ahx)_2$-CCK4 (Fig. 7B) or ^{111}In-CHX-A″-DTPA-CCK8 (Fig. 7C) showed that the tumor uptake was maintained over time while a rapid clearance from the blood was found for both compounds that resulted in low background radioactivity 24 h after injection, indicating that 24 h was the best time to evaluate these compounds. To determine the specificity of the in vivo uptake of ^{111}In-BPCA-$(Ahx)_2$-CCK4 into the tumors, a receptor competitive study was done by co-injecting the radiolabeled compound with an excess of unlabeled $(Ahx)_2$-CCK4 or gastrin (300 nmol). As shown in Table 4, the tumor-to-stomach, tumor-to-kidney and tumor-to-muscle ratios decreased by 63%, 19%, and 46%, respectively, in the presence of $(Ahx)_2$-CCK4 and by 56%, 10%, and 41% in the presence of gastrin. The significant decrease in the radioligand binding by competition with the unlabeled peptides in stomach (known to naturally express CCK-2/gastrin receptors) and tumors indicated a specific binding of the radioligand to the CCK2R. In contrast, the fact that the radioligand binding was weakly diminished in the kidney in the presence of the unlabeled peptides indicated a non-target binding of the radioligand in this organ, consistent with the fact that kidneys do not express the CCK2R and is an organ of excretion of different drugs and metabolites.

2.8. Scintigraphy imaging of the radiometal conjugates in E151A-CCK2R tumor-bearing nude mice

We then evaluated ^{111}In-CHX-A″-DTPA-$(Ahx)_2$-CCK4 and ^{111}In-BPCA-$(Ahx)_2$-CCK4 in comparison with the reference ^{111}In-CHX-A″-DTPA-CCK8 using planar scintigraphic studies of E151A-CCK2R tumor-bearing nude mice 24 h after injection of the radioactive

Table 4
Tumor-to-organ ratios 24 h post-injection of the indicated ^{111}In-radioconjugates into E151A-CCK2R tumor-bearing mice

Ratio[a]	^{111}In-CHX-A″-DTPA-CCK8	^{111}In-CHX-A″-DTPA-$(Ahx)_2$-CCK4	^{111}In-BPCA-$(Ahx)_2$-CCK4	^{111}In-BPCA-$(Ahx)_2$-CCK4+$(Ahx)_2$-CCK4[b]	^{111}In-BPCA-$(Ahx)_2$-CCK4+gastrin[c]
Tumor/Kidney	0.03 ± 0.002	0.12 ± 0.02	0.22 ± 0.03	0.18 ± 0.05	0.20 ± 0.03
Tumor/Stomach	0.90 ± 0.05	1.43 ± 0.31	4.05 ± 0.25	1.51 ± 0.10	1.80 ± 0.08
Tumor/Muscle	0.96 ± 0.02	2.12 ± 0.51	3.88 ± 0.18	2.10 ± 0.22	2.30 ± 0.21

Ahx means 6-aminohexanoic acid.
Tumor-to-organ ratios were determined from biodistribution studies (three to six experiments).
[a] After injection of the indicated ^{111}In-radioconjugates and, after co-injection of ^{111}In-BPCA-$(Ahx)_2$-CCK4 with an excess of unlabeled [b] $(Ahx)_2$-CCK4 or [c] Gastrin.

compounds (1 nmol). The images showed a marked accumulation of ^{111}In-BPCA-$(Ahx)_2$-CCK4 in the tumor that could be clearly visualized compared with ^{111}In-CHX-A″-DTPA-CCK8 and ^{111}In-CHX-A″-DTPA-$(Ahx)_2$-CCK4 (Fig. 8). A region of interest (ROI) drawn on the tumor (specific uptake) and on the muscle (non-specific uptake) enabled a tumor-to-muscle imaging ratio to be calculated, that increased from two for ^{111}In-CHX-A″-DTPA-CCK8 to six for ^{111}In-BPCA-$(Ahx)_2$-CCK4. The tumor-to-muscle imaging ratio calculated for ^{111}In- CHX-A″-DTPA-$(Ahx)_2$-CCK4 had an intermediate value of 4. These scintigraphic data are consistent with the biodistribution results and confirm that the modification introduced in the peptide part of the ligand as well as the coupling to the new chelator BPCA resulted in a higher tumor uptake of ^{111}In-BPCA-$(Ahx)_2$-CCK4 compared with ^{111}In-CHX-A″-DTPA-CCK8 and in higher tumor-to-background ratios.

The co-injection into E151A-CCK2R tumor-bearing mice of ^{111}In-BPCA-$(Ahx)_2$-CCK4 (1 nmol) and an excess of unlabeled $(Ahx)_2$-CCK4 or gastrin (300 nmol) was also evaluated by scintigraphic imaging to determine the specificity of tumor labeling. As shown in Figure 9, the CCK2R-positive tumor was clearly visualized in the left mouse after injection of ^{111}In-BPCA-$(Ahx)_2$-CCK4. In contrast, the tumor was not detected after co-injection with unlabeled $(Ahx)_2$-CCK4 or gastrin (middle and right mice), indicating specific CCK2R targeting.

3. Discussion

Taking advantage of the fact that various human cancers overexpress G protein-coupled receptors binding different peptides, such as somatostatin, MSH, VIP, neurotensin, CCK2R or gastrin receptor, radiolabeled ligands targeting these receptors have been developed within the past few years for diagnosis and therapeutic purposes.[39–41] Due to their small size, peptide-based radiopharmaceuticals are valuable tools because they can penetrate into tumors faster and more efficiently than other larger bioactive molecules, such as monoclonal antibodies.[8]

Comparisons of the renal uptake and retention of different radiolabeled peptides targeting CCK2, somatostatin, neurotensin and bombesin receptors in rats and mice have shown that ^{111}In-DTPA-CCK8 had the lowest renal uptake and ^{111}In-DTPA-minigastrin the highest compared with ^{111}In-DTPA-[Pro1,Tyr4]-bombesin, ^{111}In-DTPA-neurotensin, and ^{111}In-DTPA-octreotide.[42] These different studies revealed that a balance must be found between the contributions of the peptidic part playing on various parameters such as affinity for the target, nature, and metabolic stability, and the chelator, for which structural criteria are also essential relative to the stability of the corresponding radiochelate, and the lipophilicity, charge, size and steric hindrance of such chelates. Therefore, a suitable combination between both units needs to be found in order to lower renal accumulation and to increase the tumor uptake of the metal conjugate.

Working on these two aspects, we developed a new compound, BPCA-$(Ahx)_2$-CCK4, with improved targeting to tumors and with low renal uptake. The molecular dynamics of the CCK2R/conjugate complex helped to simulate whether an intact ligand binding pocket was conserved to maintain a high affinity binding for the conjugate. The choice of two linked 6-aminohexanoic acids as spacer enabled the chelator to be maintained outside the receptor pocket and to limit interactions with residues in the binding site, and non-specific interactions with the receptor. The fact that the indium conjugate had a high affinity for the CCK2R and stimulated a biological response with an efficacy and potency similar to the endogenous peptide indicated that no gross change in the conformation

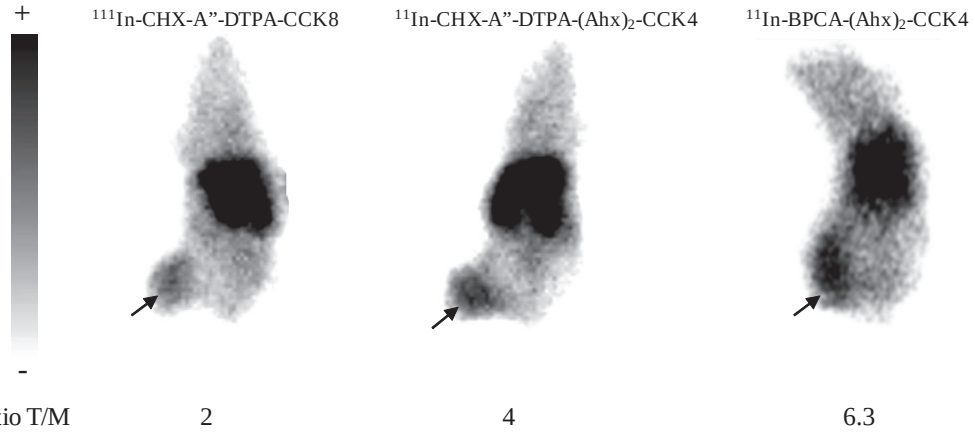

Figure 8. Scintigraphy at 24 h after injection of the indicated ^{111}In-radioconjugates into E151A-CCK2R tumor-bearing mice. For each image two elliptical Regions Of Interest (ROI) were drawn on the tumor (specific uptake) and on muscle (non-specific uptake) and corresponding counting statistics were obtained to calculate the tumor–muscle (T/M) ratios. The radioligands used were: ^{111}In-CHX-A″-DTPA-CCK8; ^{111}In-CHX-A″-DTPA-$(Ahx)_2$-CCK4 and ^{111}In-BPCA-$(Ahx)_2$-CCK4. Arrows indicate tumor uptake. The images shown are representative of three to five experiments.

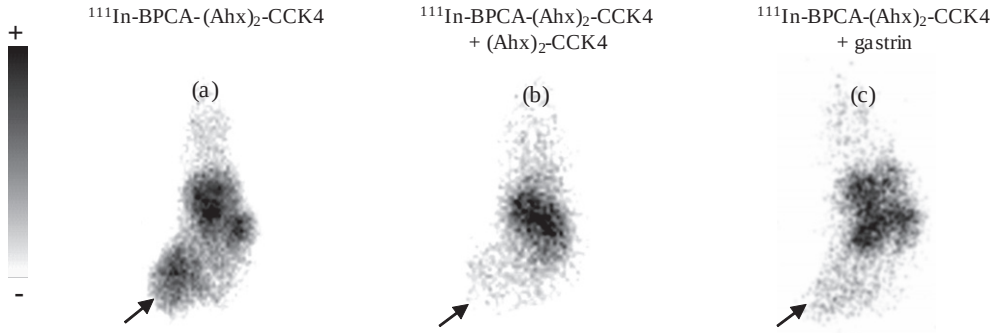

Figure 9. Scintigraphy at 24 h after injection of ^{111}In-BPCA-(Ahx)$_2$-CCK4 and in the presence of unlabeled (Ahx)$_2$-CCK4 or gastrin in E151A-CCK2R tumor-bearing mice. (a) Injection of ^{111}In-BPCA-(Ahx)$_2$-CCK4; (b), blocking was performed by co-injection of ^{111}In-BPCA-(Ahx)$_2$-CCK4 with a 300-fold excess of unlabeled (Ahx)$_2$-CCK4 and (c) blocking was performed by co-injection of ^{111}In-BPCA-(Ahx)$_2$-CCK4 with a 300-fold excess of unlabeled gastrin. Arrows indicate (a) tumor uptake and (b, c) uptake after blocking. The images shown are representative of two experiments.

of the receptor was induced by the chelator and was consistent with the molecular modeling. It is well known from molecular pharmacological investigations that agonists of these receptors induce receptor internalization.[43–45] We previously reported that the CCK2R underwent agonist-induced internalization into cells.[46] Here, we showed that our new radioligand retained the capacity to be internalized into cells after binding. The internalization of the receptor–peptide complex increases isotope accumulation inside the target cells (metabolic trapping) that is important for optimal visualization and for PRRT.[44,47] The accumulation of isotopes in the tumor allows the use of short-range emitting isotopes such as α- or β-emitters.[47]

The coupling reactions were carried out following procedures in solution on small amounts (1–10 μmol) of C-terminus protected peptides. First, CHX-A″-DTPA-CCK8 and CHX-A″-DTPA-(Ahx$_2$)-CCK4 were obtained through efficient reactions of SCN-CHX-A″-DTPA. Secondly, BPCA was coupled with a conversion level of starting peptide of 80% as measured by integrating the chromatogram of the crude mixture. Following the coupling step, a TFA cleavage of the *tert*-butyl esters protecting the carboxylate groups of the conjugated BPCA chelator was performed. It should be noted that in spite of the addition of scavengers to trap organic cations released during the reaction, there was some alkylation of the amino acid tryptophan present in the (Ahx)$_2$-CCK4 sequence. Thus, this two step procedure gave purified BPCA-(Ahx)$_2$-CCK4 conjugate at an overall yield of 20%. Therefore, the conjugation of the BPCA bifunctional agent under its protected form could be used for site specific reactions on a wide variety of unprotected peptides. Its conjugation could be also considered on peptides still having intact protection on their reactive residues, particularly the Boc-protected lysines. Moreover, the use of BPCA as a pre-organized chelator has been demonstrated as efficient based on the study of the preparation of $^{113/115}$In-complex. Indeed, in a single hour, the whole sample of BPCA-(Ahx)$_2$-CCK4 had totally disappeared when reacted with one single equivalent of $^{113/115}In^{3+}$ ion to the benefit of the corresponding indium labeled conjugate.

CHX-A″-DTPA was originally developed to increase the stability of the complex formed with Yttrium.[48] It has the advantage that it complexes the metal at room temperature as does BPCA. Coupling (Ahx)$_2$-CCK4 to BPCA resulted in a CCK derivative with several advantages compared with CHX-A″-DTPA-CCK derivatives. A 100% radiolabeling efficiency was reached after 15 min incubation of BPCA-(Ahx)$_2$-CCK4 with ^{111}In at room temperature, indicating rapid labeling kinetics. Twenty-four hours after labeling, its radiochemical purity was $\geqslant$95%, indicative of a high stability of the ^{111}In complex. Moreover, a complementary experiment performed with metal complexes ($^{113/115}$In-BPCA and $^{113/115}$In-CHX-A″-DTPA) showed that BPCA bound indium more tightly than the chelator CHX-A″-DTPA when exposed to a transchelating agent such as the transferrin. This protein, which is a serum iron transport protein, forms strong complexes with In(III) and so metal exchanges are likely to occur in vivo between radiochelates and this protein.[38] Here the relative stabilities of both complexes against transchelation appear to be in favor of the BPCA chelator. These results could certainly account for the scintigraphic results obtained with the corresponding ^{111}In-conjugate. Indeed, imaging indicates that a very good visualization of the tumor was achieved with ^{111}In-BPCA-(Ahx)$_2$-CCK4 compared with ^{111}In-CHX-A″-DTPA-CCK8, resulting in a high tumor-to-background ratio (6 vs 2) up to 24 h post-injection. This is an advantage for PRRT. Uptake of ^{111}In-BPCA-(Ahx)$_2$-CCK4 in CCK2R expressing tissues (stomach and tumor) in vivo was also found to be specific because the uptake in these tissues was significantly reduced in the presence of an excess of unlabeled (Ahx)$_2$-CCK4 or gastrin.

The scintigraphic data are in accordance with the biodistribution data that indicate a significantly higher tumor uptake of ^{111}In-BPCA-(Ahx)$_2$-CCK4 compared with ^{111}In-CHX-A″-DTPA-CCK8 and ^{111}In-CHX-A″-DTPA-(Ahx)$_2$-CCK4 and a low renal accumulation. The tumor-to-kidney ratio was sevenfold increase for ^{111}In-BPCA-(Ahx)$_2$-CCK4 (0.22) compared with ^{111}In-CHX-A″-DTPA-CCK8 (0.03) and a twofold lower accumulation of radioactivity in the kidneys was measured, which is also very favorable for their possible use in PRRT.

Moreover and interestingly, the BPCA chelator potentially offers a wide range of imaging modalities and therapeutic applications as in addition to complexing ^{111}In, as shown in the present study, BPCA may complex gadolinium for MRI applications and europium or terbium for Time-Resolved Fluorescence Spectroscopy as previously reported.[28] Finally, BPCA should have the potential to complex β-emitters like ^{90}Y for PRRT and positron emitters like ^{86}Y for diagnostic PET (Positron Emission Tomography) imaging. The success of PRRT depends on the optimization of radiation doses to tumors versus normal organs as well as on the sensitivity and performance of the diagnosis. For the same ligand, it is necessary to be able to change the type of radioisotopes, either to improve the therapeutic index of the PRRT or the diagnostic sensitivity by doing different and complementary imaging. The multimodal imaging and therapeutic applications of BPCA will be tested in future studies to complete our knowledge of this chelator that give added value.

In conclusion, we have developed a novel CCK4-based ligand conjugated to an original bipyridine-based chelator which shows a very good targeting and visualization of tumors in vivo compared with a DTPA derivative of CCK8, used as an internal control to allow a direct comparison between these radioligands. The high tumor uptake and limited renal accumulation make this CCK4-analog

a promising candidate for in vivo molecular imaging and peptide receptor radionuclide therapy of CCK2R positive tumors.

4. Experimental methods

4.1. Materials

The non-sulfated C-terminal octapeptide of cholecystokinin (indicated CCK8) and the di-1,6-hexanoïc acid C-terminal tetrapeptide of cholecystokinin ($(Ahx)_2$-CCK4) (Fig. 1) were purchased from NeoMPS (Strasbourg, France). The A″ isomer of 2-(*p*-isothiocyanatobenzyl)-cyclohexyl-diethylenetriaminepentaacetic acid (CHX-A″-DTPA) was obtained from Macrocyclics (Dallas, Texas, USA) and previously described.[31,48] The protected chelator BPCA was synthesized as previously described.[28] Triethylamine (Et_3N), trifluoroacetic acid (TFA) and triisopropylsilane (TIS) were provided by Fisher Scientific (Illkirch France). 1,1′-carbonyldiimidazole (CDI), ethanedithiol (EDT), dimethylformamide (DMF) and Chelex 100® were purchased from Sigma–Aldrich, Lyon, France. The indium(III) chloride tetrahydrate ($^{113/115}$In) was purchased from Strem Chemicals, Bischheim, France and $^{111}InCl_3$ was purchased from Covidien Imaging France (Elancourt, France, 122 MBq/ml). The human transferrin was from Sigma–Aldrich, Lyon, France. The instant thin–layer chromatography (ITLC) used was ITLC-SG® (ITLC-Silica Gel) obtained from Pall Life Sciences, Pall Corporation, NY, USA. The radiochromatogram was read with a radiochromatograph Mini-Gita® (version 2.18, Raytest, Courbevoie, France). The AG 1-X8 (formate form) was purchased from Bio-Rad Laboratories (Marnes La Coquette, France).

4.2. Molecular modeling

The molecular model of CCK9-CCK2R used was built as previously described.[33] CHX-A-DTPA-$(Ahx)_0$-CCK4, CHX-A-DTPA-$(Ahx)_1$-CCK4, and BCPA-$(Ahx)_2$-CCK4 conjugates were docked within this model by keeping the four amino acids of CCK4 interacting with the receptor residues that were characterized experimentally as important for the CCK binding.[32–35] The resulting ligand-complex models were submitted to energy minimization using 500 steps of the steepest descent followed by a conjugated gradient until the root mean square (rms) gradient was less than 0.001 kcal/mol/Å. A distant dependent dielectric term ($\varepsilon = r$) and a 20 Å non-bonded cutoff distance were chosen while the hydrogen bond involved in the conformation of the alpha transmembrane (TM) helices was preserved by applying a generic distance constraint between the backbone oxygen atoms of residue i and the backbone nitrogen atoms of residue i + 4, excluding prolines. This was performed using the Discover calculation engine with the CVFF force field (InsightII version 2000.1, Accelrys, San Diego, California, USA). The minimized coordinates of the CCK2R that were constructed using the Biopolymer module were then used as the starting point for a 150 ps at 300 K using the Verlet algorithm while the constraints used during minimization were maintained. The resulting conformations were then further minimized using 500 steps of the steepest descent followed by a conjugated gradient until the rms. gradient was less than 0.001 kcal/mol/Å.

4.3. Chemistry

Thin-layer chromatography (TLC) was carried out on Merck alumina plates with a fluorescence indicator. TLC spots were visualized by irradiation with UV light (R_f values refer to relative mobilities on the TLC plates). Column chromatography was carried out on alumina (Macherey-Nagel, Hoerdt, France, activity IV, 50–200 μm). Infrared spectrum was recorded on a Perkin–Elmer 883 spectrophotometer. The sample was applied to KBr plates and the selected characteristic absorbances are reported in cm^{-1}. Proton nuclear magnetic resonance spectra (^{1}H NMR) were recorded at 300 MHz on a Bruker AC 300 (300 MHz) spectrometer and are reported as follows: chemical shift δ in parts per million (multiplicity, number of protons, coupling constant *J* in hertz). Residual protic solvent was used as the internal reference, setting chloroform to δ 7.26. Carbon nuclear magnetic resonance spectra (^{13}C NMR) were recorded at 75 MHz on a Bruker AC 300 (300 MHz) spectrometer. Chemicals shifts are quoted in parts per million, referenced to the appropriate solvent peak, taking chloroform as δ 77.0. Electrospray (ES) mass spectra were obtained on a Perkin–Elmer SCIEX API 100 and Waters Q-TOF spectrometers.

The peptide conjugates and the $^{113/115}$In-BPCA or $^{113/115}$In-CHX-A″-DTPA complexes were analyzed by RP-HPLC using a Waters Alliance 2695 system with a PDA 2996 detector and using, respectively, a reversed-phase (RP) C_{18} column (Phenomenex Luna C18(2), 5 μm, 250 × 4.6 mm) and a RP C_8 column (Phenomenex Luna C8(2), 5 μm, 150 × 4.6 mm). In both cases, the flow rate was 1 ml/min with UV monitoring at 280 nm. For peptide conjugate analyses, the HPLC solvents were H_2O containing 0.1% TFA (solvent A) and acetonitrile (solvent B). For the analyses of indium complexes ($^{113/115}$In-BPCA or $^{113/115}$In-CHX-A″-DTPA), the HPLC solvents were 10 mM pH 4 ammonium formate buffer (solvent A) and acetonitrile (solvent B). The conjugates were analyzed using the HPLC gradient system beginning with a solvent composition of 85% A and 15% B and following a linear gradient up to 60% A:40% B from 0 to 30 min, and 60% A:40% B to 40% A:60% B from 30 to 35 min. The conjugated products were purified on a semi-preparative HPLC system, Waters Delta Prep 4000, using a RP C_{18} column (Phenomenex Luna C18(2), 5 μm, 250 × 10 mm). The flow rate was 5 ml/min with UV detection at 280 nm. The eluent and gradient were identical to the ones previously used for the analytical steps. The HPLC procedure to analyze the $^{113/115}$In-BPCA complex began with a solvent composition of 100% A followed by a linear gradient of 80% A:20% B from 0 to 18 min. The HPLC procedure to analyze the $^{113/115}$In-CHX-A″-DTPA complex began with a solvent composition of 100% A followed by a linear gradient up to 50% A:50% B from 0 to 18 min.

4.4. Preparation of BPCA 2

BPCA ester, **1**[28] (55 mg, 75.5 μmol, 1 equiv) was dissolved in 2 ml of methanol and 1 ml of an aqueous solution of potassium carbonate (10.4 mg, 75.5 μmol, 1 equiv) was added to this solution. The mixture was stirred at room temperature for 24 h and the solvent was removed under reduced pressure. The crude product was purified by column chromatography over alumina (CH_2Cl_2/MeOH 98:2) to give compound **5** (67.2 μmol, 48 mg, yield 89%). R_f (alumina, CH_2Cl_2/MeOH 98:2): 0.4. IR ν_{max}: 2978, 2931, 1732 (C=O, COO*t*Bu), 1613 (C=O, COOH), 1574, 1456, 1393, 1369. ^{1}H NMR (300 MHz, $CDCl_3$) δ: 1.39 (s, 18H, CMe_3); 1.40 (s, 18H, CMe_3); 3.39 (s, 4H, 2 CH_2CO); 3.47 (s, 4H, 2 CH_2CO); 3.92 (s, 2H, $ArCH_2$); 4.07 (s, 2H, $ArCH_2$); 7.20 (d, $J_{H5'-H4'}$ = 7.5 Hz, 1H, H5′); 7.76 (t, $J_{H4'-H5'} = J_{H4'-H3'}$ = 7.7 Hz, 1H, H4′); 7.89 (s, 1H, H5); 7.96 (d, $J_{H3'-H4'}$ = 7.7 Hz, 1H, H3′); 8.50 (s, 1H, H3). ^{13}C NMR (75 MHz, $CDCl_3$) δ: 28.0 (Me_3); 56.6, 57.0 (CH_2CO); 60.2, 60.7 ($ArCH_2N$); 82.1, 82.2 (CMe_3); 120.5, 121.0, 122.8, 124.0 (C3′, C3, C5′, C5); 138.2 (C4′); 151.2 (C4); 153.9, 155.8, 156.1, 156.7 (C2, C2′, C6, C6′); 168.6 (COOH); 171.0, 171.4 (COO*t*Bu). MS (ESI$^+$): *m*/*z* 715.6 $[M+H^+]^+$, 737.6 $[M+Na^+]^+$.

4.5. Synthesis and characterization of the peptide conjugates

For CHX-A″-DTPA-CCK8, the CCK8 peptide (4 mg, 3.8 μmol, 1 equiv) was dissolved in anhydrous DMF (190 μl). Triethylamine (Et_3N, 6 μl, 38 μmol, 10 equiv compared to the peptide) and SCN-CHX-A″-DTPA (4.5 mg, 7.6 μmol, 2 equiv compared to the peptide)

were added to this solution and the mixture stirred for 18 h at room temperature. The reaction was stopped by evaporation to dryness of the crude material. This crude product was purified by semi-preparative HPLC following the procedure described above. Analytical data of the compound are given in Table 2. Chemical purity: 96%. The CHX-A″-DTPA-$(Ahx)_2$-CCK4 compound was prepared as described above for CHX-A″-DTPA-CCK8. The reaction was carried out with the following quantities of starting materials: $(Ahx)_2$-CCK4 sequence (3.5 mg, 4.3 μmol, 1 equiv); Et_3N (6 μl, 43 μmol, 10 equiv compared to the peptide); SCN-CHX-A″-DTPA (5.2 mg, 8.7 μmol, 2 equiv compared to the peptide); DMF (220 μl). Analytical data of the compound are given in Table 2. Chemical purity: 95%. For the preparation of BPCA-$(Ahx)_2$-CCK4, the semi-protected chelator **2** (7.15 mg, 10.0 μmol, 2 equiv compared to the peptide) dissolved in DMF (150 μl) was activated with CDI (1.6 μl of a 6.25 M solution in DMF, 10 μmol, 1 equiv compared to BPCA **2**) at room temperature for 15 min and then $(Ahx)_2$-CCK4 (4 mg, 5.0 μmol, 1 equiv), dissolved in DMF (150 μl), was added. The reaction was carried out by stirring the mixture for 18 h at 40 °C and stopped by evaporation to dryness. The crude product was dissolved in a mixture of CH_2Cl_2/TFA 1:1 (TFA: 2.5 mmol, 190 μl, 500 equiv compared to the conjugate). EDT (6.6 μl, 78.7 μmol, 16 equiv compared to the conjugate) and TIS (4 μl, 20.0 μmol, 4 equiv compared to the conjugate) were then added. The mixture was incubated for 30 min at 0 °C and then stirred for 3 h at room temperature. After evaporation of the solvent, the conjugate was purified by RP-HPLC as described in Section 4.3. The analytical data of the compound are presented in Table 2. Chemical purity: 96%.

4.6. Purification of the peptide conjugates on chelating resin

This procedure was carried out for all the conjugates. Each conjugate (0.5 μmol) was dissolved in H_2O/MeOH 1:1 (500 μl) and an UV analysis of this solution was recorded. Chelex 100® resin was added (20 mg), the mixture stirred for 1 h at room temperature and then centrifuged. The supernatant was recovered and an UV analysis done to ensure an efficient recovery.

4.7. Preparation and characterization of the $^{113/115}$In-labeled conjugates

Procedure A: Labeling of conjugates with $^{113/115}$In: this procedure was carried out on an analytical amount of conjugates (0.04 μmol). To obtain $^{113/115}$In-CHX-A″-DTPA-$(Ahx)_2$-CCK4: the conjugate CHX-A″-DTPA-$(Ahx)_2$-CCK4 (4.0 μl of a 10 mM aq solution, 0.04 μmol, 1 equiv) was complexed with $^{113/115}InCl_3.4H_2O$ (3.3 μl of a 12 mM aq solution, 0.04 μmol, 1 equiv compared to the conjugate) in a 0.1 M sodium acetate buffer pH 5 (AcONa, 72 μl) or in H_2O (72 μl) for mass spectrometric analysis. The mixture was stirred for 1 h at room temperature. Half of the mixture was analyzed by HPLC and the other half by ESI-MS spectrometry: m/z, $[M+H^+]_{calculated} = 1511.5 - m/z$, $[M+H^+]_{observed} = 1511.8$. Retention time: $R_t = 27.5$ min. Chemical purity: 97%. The $^{113/115}$In-BPCA-$(Ahx)_2$-CCK4 labeled conjugate was prepared from BPCA-$(Ahx)_2$-CCK4 as described above with the following quantities of products: BPCA-$(Ahx)_2$-CCK4 conjugate (4 μl of a 10 mM aq solution, 0.04 μmol), $^{113/115}InCl_3{\cdot}4H_2O$ (3.3 μl of a 12 mM aq solution, 0.04 μmol), 0.1 M pH 5 AcONa or H_2O (72 μl). ESI-MS spectrometry: m/z, $[M-H^+]_{calculated} = 1387.5 - m/z$, $[M-H^+]_{observed} = 1387.2$. Retention time: $R_t = 22.25$ min. Chemical purity: 99%.

Procedure B: Stability of $^{113/115}$In-complexes to transchelation: for a simpler analysis of the results, this procedure was applied to the unconjugated chelators BPCA and CHX-A″-DTPA. Labeling of BPCA and CHX-A″-DTPA with $^{113/115}$In ($InCl_3.4H_2O$) was done by adding a solution of the chelator in water (0.60 μmol, 1 equiv) to an aqueous solution of indium chloride (0.66 μmol, 1.1 equiv). The mixture was stirred at room temperature for 1 h. A part (0.4 μmol) of the resulting stock solution (40 mM in complex) was then diluted (1/20) in a solution of transferrin in a 50 mM HEPES buffer pH 7.3 (0.25 g/100 ml), and the other part (0.2 μmol) was treated as a T_0 reference point. The major aliquot was incubated at 37 °C and samples were taken at $T_1 = 2.5$ h and $T_2 = 5.5$ h for RP-HPLC analyses. Prior to the analyses, the protein was removed by precipitation with cold ethanol (200 μl added to samples of the same volume). The supernatants were recovered, dried under reduce pressure and dissolved in water (100 μl) for analysis. HPLC characterization of the stability of the indium complexes was performed following the procedures given above in Section 4.3. Integrations of the peaks of the complexes enabled the percentages present to be determined as a function of the time of incubation in the presence of the transchelating agent, that is, the transferrin. For the In-BPCA complex: $R_t = 8.5$ min, T_0 (100%), T_1 (89%), T_2 (71%); for the In-CHX-A″-DTPA: $R_t = 13.8$ min, T_0 (100%), T_1 (45%), T_2 (23%).

4.8. Radiolabeling and quality control the radiometal conjugates

The pH of $^{111}InCl_3$ (500 μl) was adjusted to 5 with 1 M NaOH and 10 nM of the conjugates added. After incubating the reaction mixture for 1 h at 25 °C, the RCP was determined by ITLC using 0.1 M sodium citrate buffer pH 5 as eluent. Free ^{111}In migrated at the solvent front (9 cm) and ^{111}In-labeled conjugates stayed at the deposit (2 cm). The percentage of ^{111}In-labeled peptide was determined with the radiochromatograph Mini-Gita®. For radiolabeling stability studies, tests were performed at different times after labeling.

4.9. Cell culture

The NIH-3T3 fibroblast cell line stably expressing a tumorigenic mutant of the CCK2R (CCK2R-E151A cells, clone M1)[19] was cultured in DMEM supplemented with 10% fetal bovine serum (FCS), 2 mM L-glutamine and 0.5% penicillin/streptomycin. COS cells (LGC standards, UK) were cultured in a similar medium supplemented with 5% FCS. All cell lines were grown in a humidified atmosphere containing 5% CO_2 at 37 °C and split when they were 80% confluent.

4.10. Transfection of the CCK2R and CCK1R into COS cells

Two micrograms of the CCK2R or CCK1R cDNAs were transiently transfected into COS cells using the DEAE/Dextran method as described previously.[35]

4.11. Inositol phosphates measurement

The assays were performed as previously described.[35] Briefly, 24 h after transfection, COS cells were transferred to 24-well culture plates (100,000 cells/well) and incubated overnight in DMEM containing 2 μCi/well of myo-2-[^{3}H]inositol (18.6 Ci/mmol) (GE healthcare, France). Following the aspiration of the medium, the cells were incubated at 37 °C for 20 min with 1 ml of DMEM containing 20 mM LiCl. The cells were then washed with IP buffer pH 7.4 (20 mM Hepes, 135 mM NaCl, 2 mM $CaCl_2$, 1.2 mM $MgSO_4$, 1 mM EGTA, 10 mM LiCl, 11 mM glucose and 0.5% BSA) and then incubated for 1 h at 37 °C with IP buffer containing the indicated concentrations of peptide derivatives. The reaction was stopped by adding 1 ml of methanol/HCl to each well and the contents transferred to an AG 1-X8 column (formate form). Each column was washed twice with 3 ml water followed by 2 ml of 5 mM

sodium tetraborate/60 mM sodium formate. Total inositol phosphates (IP) were eluted from the columns with 2 ml of 1 M ammonium formate/100 mM formic acid. [^{3}H]myo-inositol phosphate radioactivity was counted in a liquid scintillation counter (Packard, Downers Grove, IL). The EC_{50} were calculated using GraphPad Prism Program Software.

4.12. Binding assays

The experiments were performed as previously described.[35] Twenty-four hours after the transfer of the cells to 24-well plates (100,000 cells/well), the cells were incubated for 60 min (time determined to reach binding equilibrium) with increasing amounts of ^{111}In-CHX-A″-DTPA-$(Ahx)_2$-CCK4 in DMEM medium containing 0.1% BSA at 37 °C. Non-specific binding was measured under similar conditions in the presence of 1 μM unlabeled CCK8 and was always less than 10% of the total binding. The reaction was stopped by washing the cells three times with cold PBS containing 4% BSA. The cells were then collected with 0.5 ml of 0.1 N NaOH added to each well. The radioactivity was detected in a Wallac Wizards® γ counter. Assays were carried out in duplicate in two separate experiments. Data were analyzed using the GraphPad Prism Program Software.

4.13. Internalization studies

Cells were prepared as mentioned above and then incubated with 100 kBq ^{111}In-BPCA-$(Ahx)_2$-CCK4 at 37 °C for various time intervals between 5 and 60 min. At the times indicated, the cells were rapidly washed twice with PBS containing 4% BSA and exposed to 0.5 M KSCN for 10 min at room temperature. Cell-associated radioactivity was measured in a γ counter after solubilizing the cells with 1 ml of 1% SDS. In all cases, parallel incubations were performed in the presence of 1 μM unlabeled CCK8 to determine non-specific binding at each time point. Internalized receptor was defined as cell-associated radioactivity after stripping and expressed as the percent of the total specific binding.

4.14. Biodistribution studies

Swiss nu/nu nude mice were purchased from Charles River Laboratories (France) and maintained in specific pathogen-free conditions. All of the procedures for animal care and use of laboratory animals were carried out according to the guidelines of our institution and followed the general regulations governing animal experimentation (Directive no. 86/609/EEC Art. 10). Exponentially growing CCK2R-E151A cells were harvested, washed twice in PBS, and resuspended in PBS. Tumors were implanted by subcutaneous transplantation of 150 μl of 2×10^6 CCK2R-E151A cells into the thighs of the mice (6 weeks old). When the average volume of tumors reached 1000 mm^3, 100 μl of ^{111}In-CCK-derivatives (1 nmol, around 8 MBq) were injected intravenously into the tail vein of the mice. Specific labeling was evaluated by co-injecting ^{111}In-BPCA-$(Ahx)_2$-CCK4 (1 nmol, around 8 MBq) with an excess of unlabeled $(Ahx)_2$-CCK4 peptide or gastrin (300 nmol). At the indicated time after injection, imaging or biodistribution studies were performed. For the biodistribution studies, mice were sacrificed by cervical dislocation. Blood, spleen, stomach, bowel, kidneys, gallbladder, liver, lungs, heart, muscle, and tumor were collected, weighted and counted in a Wallac Wizards® γ counter. Data were calculated as percentage of the injected dose per gram of tissue (% ID/g).

4.15. Scintigraphy imaging studies

At the indicated time after injection as described above, mice were anesthetized by an intramuscular injection with a mixture of ketamine 50 mg/ml, xylazine 19 mg/ml, and NaCl 0.9% (33:6.3:60.7). Planar acquisition was performed over 40 min using a gamma camera (Millennium VG® or Infinia®- GEHC, US) equipped with medium energy high resolution collimators. Image analysis was done on a Xeleris workstation (GEHC Waukesha, US). For each image, two elliptical regions of interest (ROI) were drawn: the first surrounding the tumor (specific uptake) and the second, the muscle (non-specific uptake) and corresponding counting statistics extracted (maximum and mean of the counts and standard deviation). The number of pixels was the same for each image. After imaging, the mice were sacrificed by cervical dislocation.

Acknowledgments

We would like to thank Dr. Nadine Leygue for the preparation of the protected BPCA compound, Dr. Olivier Caselles, head of Medical Physics, for SPECT optimization protocol for small animal imaging and Dr. Pierre Canal for his help. This work was supported by an internal Grant from INSERM, the Institut Claudius Regaud, the Université Paul Sabatier (Toulouse) and the Conseil Regional Midi-Pyrénées. S.D. has been supported by a Grant from 'La Ligue contre le cancer'. Dr. S.S.-P. is in charge of research at the CNRS.

Supplementary data

Supplementary data (HPLC chromatograms and ESI-MS spectra of peptide conjugates CHX-A″-DTPA-CCK8, CHX-A″-DTPA-$(Ahx)_2$-CCK4 and BPCA-$(Ahx)_2$-CCK4) associated with this article can be found, in the online version, at doi:10.1016/j.bmc.2010.05.031.

References and notes

1. Reubi, J. C. *Q. J. Nucl. Med.* **1997**, *41*, 63.
2. Heppeler, A.; Froidevaux, S.; Eberle, A. N.; Maecke, H. R. *Curr. Med. Chem.* **2000**, *7*, 971.
3. Krenning, E. P.; Kwekkeboom, D. J.; Bakker, W. H.; Breeman, W. A.; Kooij, P. P.; Oei, H. Y.; van Hagen, M.; Postema, P. T.; de Jong, M.; Reubi, J. C., et al *Eur. J. Nucl. Med.* **1993**, *20*, 716.
4. Lebtahi, R.; Cadiot, G.; Sarda, L.; Daou, D.; Faraggi, M.; Petegnief, Y.; Mignon, M.; le Guludec, D. *J. Nucl. Med.* **1997**, *38*, 853.
5. Behe, M.; Behr, T. M. *Biopolymers* **2002**, *66*, 399.
6. Gotthardt, M.; Behe, M. P.; Grass, J.; Bauhofer, A.; Rinke, A.; Schipper, M. L.; Kalinowski, M.; Arnold, R.; Oyen, W. J.; Behr, T. M. *Endocr. Relat. Cancer* **2006**, *13*, 1203.
7. Kwekkeboom, D. J.; Reubi, J. C.; Lamberts, S. W.; Bruining, H. A.; Mulder, A. H.; Oei, H. Y.; Krenning, E. P. *J. Clin. Endocrinol. Metab.* **1993**, *76*, 1413.
8. Okarvi, S. M. *Cancer Treat. Rev.* **2008**, *34*, 13.
9. Steigerwalt, R. W.; Williams, J. A. *Regul. Pept.* **1984**, *8*, 51.
10. Caplin, M.; Khan, K.; Savage, K.; Rode, J.; Varro, A.; Michaeli, D.; Grimes, S.; Brett, B.; Pounder, R.; Dhillon, A. *J. Hepatol.* **1999**, *30*, 519.
11. McWilliams, D. F.; Watson, S. A.; Crosbee, D. M.; Michaeli, D.; Seth, R. *Gut* **1998**, *42*, 795.
12. Savage, K.; Waller, H. A.; Stubbs, M.; Khan, K.; Watson, S. A.; Clarke, P. A.; Grimes, S.; Michaeli, D.; Dhillon, A. P.; Caplin, M. E. *Int. J. Oncol.* **2006**, *29*, 1429.
13. Smith, J. P.; Shih, A. H.; Wotring, M. G.; McLaughlin, P. J.; Zagon, I. S. *Int. J. Oncol.* **1998**, *12*, 411.
14. Reubi, J. C.; Schaer, J. C.; Waser, B. *Cancer Res.* **1997**, *57*, 1377.
15. Blackmore, M.; Hirst, B. H. *Br. J. Cancer* **1992**, *66*, 32.
16. Caplin, M.; Khan, K.; Grimes, S.; Michaeli, D.; Savage, K.; Pounder, R.; Dhillon, A. *Dig. Dis. Sci.* **2001**, *46*, 1356.
17. Grabowska, A. M.; Watson, S. A. *Cancer Lett.* **2007**, *257*, 1.
18. Oikonomou, E.; Buchfelder, M.; Adams, E. F. *Neuropeptides* **2008**, *42*, 255.
19. Gales, C.; Sanchez, D.; Poirot, M.; Pyronnet, S.; Buscail, L.; Cussac, D.; Pradayrol, L.; Fourmy, D.; Silvente-Poirot, S. *Oncogene* **2003**, *22*, 6081.
20. Paillasse, M. R.; de Medina, P.; Amouroux, G.; Mhamdi, L.; Poirot, M.; Silvente-Poirot, S. *J. Lipid Res.* **2009**, *50*, 2203.
21. Gotthardt, M.; Behe, M. P.; Beuter, D.; Battmann, A.; Bauhofer, A.; Schurrat, T.; Schipper, M.; Pollum, H.; Oyen, W. J.; Behr, T. M. *Eur. J. Nucl. Med. Mol. Imaging* **2006**, *33*, 1273.
22. Behr, T. M.; Behe, M. P. *Semin. Nucl. Med.* **2002**, *32*, 97.
23. Kwekkeboom, D. J.; Bakker, W. H.; Kooij, P. P.; Erion, J.; Srinivasan, A.; de Jong, M.; Reubi, J. C.; Krenning, E. P. *Eur. J. Nucl. Med.* **2000**, *27*, 1312.
24. Harrison, A.; Walker, C. A.; Parker, D.; Jankowski, K. J.; Cox, J. P.; Craig, A. S.; Sansom, J. M.; Beeley, N. R.; Boyce, R. A.; Chaplin, L., et al *Int. J. Radiat. Appl. Instrum. B* **1991**, *18*, 469.

25. Aloj, L.; Caraco, C.; Panico, M.; Zannetti, A.; Del Vecchio, S.; Tesauro, D.; De Luca, S.; Arra, C.; Pedone, C.; Morelli, G.; Salvatore, M. *J. Nucl. Med.* **2004**, *45*, 485.
26. Behe, M.; Becker, W.; Gotthardt, M.; Angerstein, C.; Behr, T. M. *Eur. J. Nucl. Med. Mol. Imaging* **2003**, *30*, 1140.
27. Good, S.; Walter, M. A.; Waser, B.; Wang, X.; Muller-Brand, J.; Behe, M. P.; Reubi, J. C.; Maecke, H. R. *Eur. J. Nucl. Med. Mol. Imaging* **2008**, *35*, 1868.
28. Havas, F.; Danel, M.; Galaup, C.; Tisnès, P.; Picard, C. *Tetrahedron Lett.* **2007**, *48*, 999.
29. Sun, Y.; Anderson, C. J.; Pajeau, T. S.; Reichert, D. E.; Hancock, R. D.; Motekaitis, R. J.; Martell, A. E.; Welch, M. J. *J. Med. Chem.* **1996**, *39*, 458.
30. Havas, F.; Leygue, N.; Danel, M.; Mestre, B.; Galaup, C.; Picard, C. *Tetrahedron* **2009**, *65*, 7673.
31. Clifford, T.; Boswell, C. A.; Biddlecombe, G. B.; Lewis, J. S.; Brechbiel, M. W. *J. Med. Chem.* **2006**, *49*, 4297.
32. Gales, C.; Poirot, M.; Taillefer, J.; Maigret, B.; Martinez, J.; Moroder, L.; Escrieut, C.; Pradayrol, L.; Fourmy, D.; Silvente-Poirot, S. *Mol. Pharmacol.* **2003**, *63*, 973.
33. Paillasse, M. R.; Deraeve, C.; de Medina, P.; Mhamdi, L.; Favre, G.; Poirot, M.; Silvente-Poirot, S. *Mol. Pharmacol.* **2006**, *70*, 1935.
34. Silvente-Poirot, S.; Escrieut, C.; Gales, C.; Fehrentz, J. A.; Escherich, A.; Wank, S. A.; Martinez, J.; Moroder, L.; Maigret, B.; Bouisson, M.; Vaysse, N.; Fourmy, D. *J. Biol. Chem.* **1999**, *274*, 23191.
35. Silvente-Poirot, S.; Escrieut, C.; Wank, S. A. *Mol. Pharmacol.* **1998**, *54*, 364.
36. Behr, T. M.; Behe, M.; Angerstein, C.; Gratz, S.; Mach, R.; Hagemann, L.; Jenner, N.; Stiehler, M.; Frank-Raue, K.; Raue, F.; Becker, W. *Clin. Cancer Res.* **1999**, *5*, 3124s.
37. Sabbatini, N.; Guardigli, M.; Manet, I.; Bolleta, F.; Ziessel, R. *Inorg. Chem.* **1994**, *33*, 955.
38. Harris, W.; Chen, Y.; Wein, K. *Inorg. Chem.* **1994**, *33*, 4991.
39. de Visser, M.; Verwijnen, S. M.; de Jong, M. *Cancer Biother. Radiopharm.* **2008**, *23*, 137.
40. Reubi, J. C.; Macke, H. R.; Krenning, E. P. *J. Nucl. Med.* **2005**, *46*, 67S.
41. Behr, T. M.; Gotthardt, M.; Barth, A.; Behe, M. Q. *J. Nucl. Med.* **2001**, *45*, 189.
42. Melis, M.; Krenning, E. P.; Bernard, B. F.; de Visser, M.; Rolleman, E.; de Jong, M. *Nucl. Med. Biol.* **2007**, *34*, 633.
43. Cescato, R.; Schulz, S.; Waser, B.; Eltschinger, V.; Rivier, J. E.; Wester, H. J.; Culler, M.; Ginj, M.; Liu, Q.; Schonbrunn, A.; Reubi, J. C. *J. Nucl. Med.* **2006**, *47*, 502.
44. Bodei, L.; Paganelli, G.; Mariani, G. *J. Nucl. Med.* **2006**, *47*, 375.
45. Koenig, J. A.; Edwardson, J. M. *Trends Pharmacol. Sci.* **1997**, *18*, 276.
46. Pohl, M.; Silvente-Poirot, S.; Pisegna, J. R.; Tarasova, N. I.; Wank, S. A. *J. Biol. Chem.* **1997**, *272*, 18179.
47. Zhang, H.; Chen, J.; Waldherr, C.; Hinni, K.; Waser, B.; Reubi, J. C.; Maecke, H. R. *Cancer Res.* **2004**, *64*, 6707.
48. Camera, L.; Kinuya, S.; Garmestani, K.; Wu, C.; Brechbiel, M. W.; Pai, L. H.; McMurry, T. J.; Gansow, O. A.; Pastan, I.; Paik, C. H., et al *J. Nucl. Med.* **1994**, *35*, 882.